Astron. Astrophys. 360, 1126–1138 (2000)

ASTRONOMY AND ASTROPHYSICS

Linear and nonlinear statistical analysis of narrow-band dm-spikes observed during the June 15, 1991 flare

H. Mészárosová[1], **M. Karlický**[1], **A. Veronig**[2], **P. Zlobec**[3], **and M. Messerotti**[3]

[1] Astronomical Institute of the Academy of Sciences of the Czech Republic, 25165 Ondřejov, Czech Republic (hana@asu.cas.cz)
[2] Institute of Astronomy, University of Graz, Universitätsplatz 5, 8010 Graz, Austria
[3] Trieste Astronomical Observatory, Via G.B. Tiepolo 11, 34131 Trieste, Italy

Received 25 October 1999 / Accepted 6 April 2000

Abstract. Narrow-band dm-spikes observed during the June 15, 1991 flare are statistically analysed. The character of their frequency distributions at 237, 327, 408 and 610 MHz in both L- and R-handed circular polarizations is studied. While for the complete time intervals no simple distributions of spikes (either exponential or power-law) are recognized, for shorter intervals both exponential and power-law distributions are observed. No significant difference is found in the distributions for L- and R-polarized data. Further analysis reveals that spikes appearing in dense groups and with high intensities preferentially have exponential distributions, while the sparse spikes with lower intensities are rather characterized by power-law distribution functions with high exponents. Groups of independent spikes (cases with low rates and low intensities) have power-law distributions trend in agreement with the coherent spike mechanisms. Tests are provided regarding statistical analyses. The nonlinear analysis reveals that the degree of complexity of the system varies. It decreases when the attractor dimensions and the Lyapunov exponents assume smaller values, which happens when very strong spikes are present. The changing characteristics of the statistical parameters are probably the result of a mutual interaction in the source environment or a product of propagation conditions.

Key words: acceleration of particles – methods: data analysis – methods: statistical – Sun: flares – Sun: magnetic fields – Sun: radio radiation

1. Introduction

An exceptionally high brightness temperature ($T_b \approx 10^{15}$ K) and a very short duration ($\leq$ 0.1 s) are the main reasons that narrow-band dm-spikes are studied so intensively (see the review by Benz 1986). Observational characteristics of these bursts were presented in many papers (e.g. Slottje 1981; Karlický 1984; Stähli & Magun 1986). The theoretical models can be divided in two groups: in the first group the narrow-band dm-spikes are considered as radio manifestations of plasma emission and acceleration processes (Kuijpers et al. 1981; Tajima et al. 1990; Wentzel 1991), in the second group they are explained as generated by the electron-cyclotron maser mechanism (Holman et al. 1980; Melrose & Dulk 1982; Aschwanden 1990; Fleishman & Yastrebov 1994). It was also suggested that the dm-spikes are due to the radio emission of superthermal electrons accelerated in turbulent MHD cascading waves generated in magnetic field reconnection outflows (Karlický et al. 1996).

To obtain more information about the spike emission mechanism, several studies based on statistical analysis were carried out. While in the previous papers the inner mutual relationship among spikes or the relationship of spikes to other radio bursts were analysed (Schwarz et al. 1993; Benz et al. 1996), in the recent paper by Aschwanden et al. (1998) the frequency distributions of spikes were studied. In that paper it is reported that the frequency distributions of dm-spikes fit an exponential function, in contrast to the power-law trend expected for the generally proposed coherent emission mechanisms. A nonlinear saturation of the coherent emission mechanism at a fixed amplification factor for all the spikes was suggested to reconcile the found exponential distributions with the spike theory.

The above aspects are just the argument of this paper. We are mainly interested in the character of the frequency distributions and in the degree of complexity of narrow-band dm-spikes. We therefore analysed the group of spikes observed during the June 15, 1991 flare, as in this case an exceptionally long series of such bursts was observed (16 minutes – from 08:20:00 to 08:36:00 UT) and some parameters of these spikes are already determined (Zlobec & Karlický 1998).

2. Statistical methods

Four independent statistical methods comprising linear as well as nonlinear approaches were used for the global and the detailed analysis of spikes: the standard method, the subinterval maxima distribution method, fractal dimensions and recurrence plots. The methods are described in the following subsections.

Send offprint requests to: H. Mészárosová (hana@asu.cas.cz)

2.1. Linear time series analysis

2.1.1. Standard method

First, within the studied interval of radio data, all relative maxima and minima were determined. Then the distributions of these maxima in a selected number of bins between the absolute maximum and minimum were computed and plotted on a log-log scale. Finally, the distribution type was determined by fitting a power-law and an exponential function, judging the goodness of the fits by a reduced χ^2 test.

Furthermore the number of spikes in the specified intervals was evaluated as the number of maxima above a given flux level. This level was determined as 1.15 times the minimum radio flux or equal to the turnover defined as the distribution maximum (Aschwanden et al. 1998). Then, knowing the number of spikes, their rate per second was derived.

2.1.2. Sub-interval maxima distribution method

The whole interval considered was divided into many short subintervals lasting a definite time, and in each of them the absolute maximum was determined. In this method the free parameter is the number of points per sub-interval. For our study subintervals with 2, 10, 20, 30, 40, 50, 60 and 80 samples (i.e. they are lasting from 0.04 to 1.60 s) were used. Afterwards the distributions of these maxima normalized to the sub-interval number were represented in log-log plots and the distribution type was determined as in the previous method.

2.1.3. Computation of the reduced χ^2 test function

The results obtained by the methods described in previous paragraphs were fitted by exponential and power-law functions. To decide what fitting is more suitable and statistically correct we used the following reduced χ^2 test function (Press et al. 1992; Bevington 1969):

$$\chi^2 = \left(\frac{1}{n_{\rm deg}} \sum_i \frac{({\rm N}_i - n_i)^2}{n_i} \right)^{1/2} \quad i = 1, ..., n_{\rm bins} \,, \tag{1}$$

where N_i is the observed number of events in the i-th bin and n_i denotes the theoretically predicted number of events in the i-th bin (i.e. from the power-law or exponential fits). $n_{\rm bins}$ gives the number of bins in the fitted histograms, $n_{\rm deg}$ denotes the degrees of freedom, given by $n_{\rm deg} = n_{\rm bins} - n_{\rm par}$, with $n_{\rm par}$ the number of parameters of the fitted functions. In our case for both power-law and exponential functions $n_{\rm par} = 2$. The following rule is used for an estimate of how appropriate the considered fits are:

(a) If the reduced χ^2 is near unity, within an approximate range of $0.9 \lesssim \chi^2 \lesssim 1.1$, the model can be considered as consistent with the data (even if this cannot provide a full proof of the correctness of the model).
(b) If the reduced χ^2 is significantly higher than unity, than the model can be considered as not consistent with the data.
(c) If the reduced χ^2 is much smaller than unity, this means that the reduced χ^2 is not sensitive to the fit and no statement can be made whether the model is consistent or inconsistent with the data.

Therefore, to decide between two models it is necessary that one model gives a good fit ($0.9 \lesssim \chi^2 \lesssim 1.1$) and simultaneously the other gives a significantly worse fit (for example $\chi^2 > 1.2$).

2.2. Nonlinear time series analysis

Nonlinear time series analysis, based on the theory of deterministic chaos, has become an important tool for understanding complex dynamics from observational time series (for recent reviews see Grassberger et al. 1991; Abarbanel 1996; Kantz & Schreiber 1997; Schreiber 1999). Specifically, it offers statistical descriptions and explanations for irregular time series, which, nevertheless, might not be governed by a (purely) stochastic process.

2.2.1. Fractal dimensions

The dimension of an attractor, i.e., the limit set of trajectories once all transient phenomena have faded out, indicates the number of independent variables needed to describe the related dynamical system. Based on this fact, the determination of fractal dimensions might enable us to establish if the system is deterministic or stochastic. Calculating fractal dimensions of time series, the correlation dimension, introduced by Grassberger & Procaccia (1983), is commonly used. We focus our attention on a local equivalent, the so-called local pointwise dimension, since it enables us to cope with non-stationary data and can provide statistical information even in cases in which pure determinism in the data cannot be ascertained (see Veronig et al. 2000).

To reconstruct the phase space of a dynamical system from a measured time series, we applied the techniques of time delayed coordinates (Takens 1981). From a given one-dimensional time series $\{x_i\}$ an m-dimensional new phase space $\{\boldsymbol{\xi}_i\}$, the so-called embedding space, is built up by the prescription

$$\boldsymbol{\xi}_i = \{x(t_i),\ x(t_i + \tau),\ \ldots\ , x(t_i + (m-1)\tau)\} \,, \tag{2}$$

with the time delay τ. The choice of the delay parameter τ is quite critical, as for time series with finite length and accuracy it strongly affects the suitability of the reconstructed coordinates. We use the first minimum of the mutual information (Fraser & Swinney 1986), which is a kind of nonlinear generalization of the auto-correlation function.

The definition of the local pointwise dimension is based on the probability $p_i(r)$ to find points in a neighbourhood of the point $\boldsymbol{\xi}_i$ with size r :

$$p_i(r) = \frac{1}{\mathrm{N}_{\rm pairs}} \sum_{\substack{j=1 \\ |j-i| \geq W}}^{\mathrm{N}} \Theta(r - \|\boldsymbol{\xi}_i - \boldsymbol{\xi}_j\|) \,, \tag{3}$$

where N denotes the overall number of data points, $\mathrm{N}_{\rm pairs}$ gives the number of pairs of points in the sum, Θ is the Heaviside step

function, and the correction term W excludes temporally correlated points from the sum and should at least cover all points within the auto-correlation time (Theiler 1986). For small distances r, $p_i(r)$ is expected to scale with a power of r, and for sufficiently high embedding dimensions m, the scaling exponent $D_p(\boldsymbol{\xi}_i)$ converges to the local pointwise dimension at point $\boldsymbol{\xi}_i$:

$$p_i \propto r^{D_p(\boldsymbol{\xi}_i)}, \quad D_p(\boldsymbol{\xi}_i) = \lim_{r\to 0} \frac{\ln p_i(r)}{\ln r}. \tag{4}$$

On the one hand, the $D_p(\boldsymbol{\xi}_i)$ are a function of the position $\boldsymbol{\xi}_i$ on the attractor, on the other hand the local dimensions can be interpreted as a function of time, $D_p(t_i)$, as they reflect the temporal order, in which the points $\boldsymbol{\xi}_i$ on the attractor are covered by the dynamics.

2.2.2. Recurrence plots

The basic idea of recurrence plots is that dots (i, j) are plotted in an N × N array, whenever point $\boldsymbol{\xi}_i$ is sufficiently close to point $\boldsymbol{\xi}_j$ (Eckmann et al. 1987). As the i, j are in fact times, a recurrence plot describes time correlation information and is therefore a graphical analysis tool which gives inferences on the dynamics of the system. For instance, on global scales a recurrence plot makes it possible to detect non-stationarities in the data, on local scales it gives information on local Lyapunov exponents.

Chaotic systems are characterized by a high sensitivity to initial conditions. An initially infinitesimal perturbation will grow exponentially, and the Lyapunov exponent quantifies the growth rate. A positive, finite value of the leading Lyapunov exponent stands for an exponential divergence of nearby trajectories under the dynamics of the system, which defines a chaotic system. Moreover, the leading Lyapunov exponent is related to the time of predictability of the system: large Lyapunov exponents are related to short times of predictability, and vice versa.

In a recurrence plot the presence of line segments parallel to the diagonal indicates intervals in the time series which are governed by finite local Lyapunov exponents: longer lines are related to smaller and shorter lines to larger local Lyapunov exponents. This is simply understood by the method of construction of a recurrence plot, which is basically a visualization of near neighbours in phase space. Lines parallel to the diagonal indicate intervals in the time series, in which near neighbours remain near neighbours under the dynamics of the system: the longer the lines, the smaller the exponential divergence rate of the corresponding trajectories, i.e. the Lyapunov exponents. For the limit case of periodic systems lines parallel to the diagonal are stretched over the whole recurrence plot, and their constant spacing is determined by the period.

The recurrence plot of time series with a drift is dominated by a fading away from the diagonal, which results from the fact that dots far away from the diagonal belong to points in the time series with large temporal distances, and with increasing time lag the drift enlarges the distance between such points in phase space, whereas dots near the diagonal belong to points which are close in time and therefore less affected by the drift. This leads to the phenomenon that for times series with a drift most of the near neighbours, i.e. black dots in the recurrence plot, are located near the diagonal.

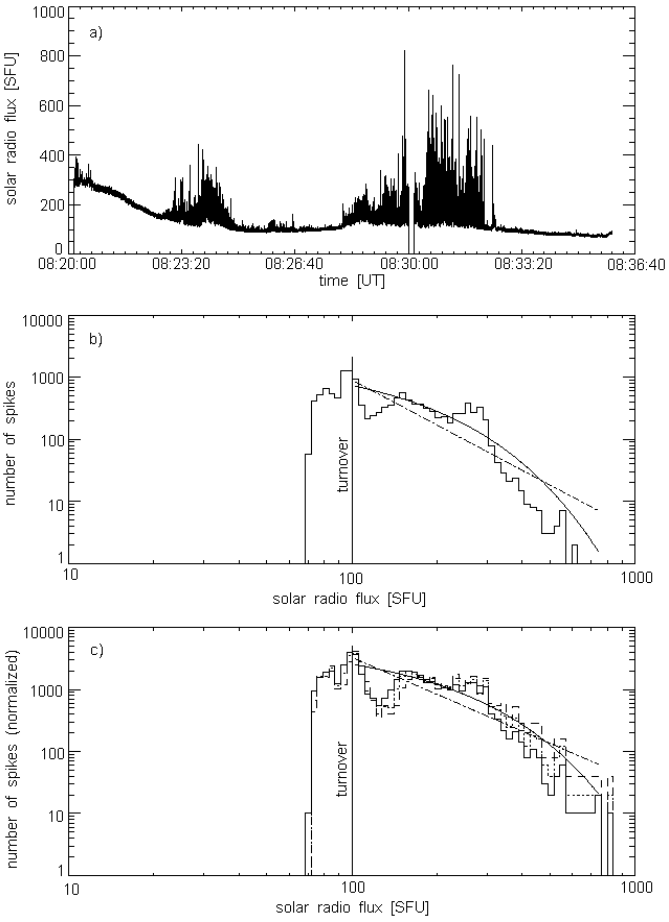

Fig. 1. a Radio flux record observed at 408 MHz (L-handed polarization) in the whole, 16 minute long interval. **b** Global distribution obtained by the standard method. **c** Global distributions obtained by the sub-interval method where solid, dotted and dashed lines stand for 10, 20 and 40 points, respectively. Solid and dashed-dot lines (in **b**, **c**) represent the exponential and power-law fits, respectively.

3. Results

During the June 15, 1991 flare (Karlický 1992; Akimov et al. 1996) an exceptionally long period with narrow-band dm-spikes was observed (Zlobec & Karlický 1998). The spikes were recorded with a digitization rate of 50 Hz at the Trieste Astronomical Observatory at 237, 327, 408 and 610 MHz in both circular polarizations (left (L) and right(R)) in the time interval 08:20:00−08:36:00 UT. This unique data set was used for the following statistical analyses.

3.1. Global study

The frequency distributions of the complete intervals were determined. The same statistical method was used for the R- as

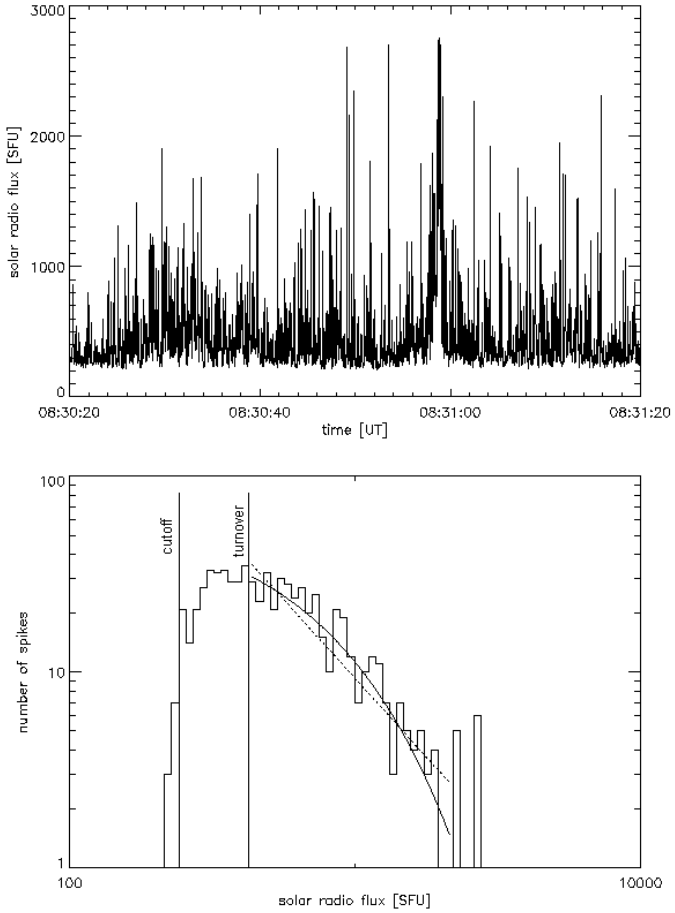

Fig. 2. Example of a 1 minute interval with dense spikes observed at 610 MHz, L-polarized data and the corresponding distributions. The solid line corresponds to the better fit: in this case exponential.

well as for the L-polarized components. The results for both polarizations are similar: a) identical results were obtained for the intervals when the polarization was about zero; b) a small but non-essential difference was found in the intervals when the polarization was increasing (for the polarization trend – see Zlobec & Karlický 1998).

As an example the plot of the 408 MHz L-polarized emission (Fig. 1a) is presented. The frequency distributions obtained with the standard method and with the sub-interval maxima distribution method are shown in Figs. 1b and 1c. Sub-intervals formed by 10, 20 and 40 points were considered. The results shown in Figs. 1b and 1c are very similar, mainly for sub-intervals corresponding to 10 points. Although the values of the χ^2 test function are lower for the exponential fit than for the power-law fit, none of the distribution models fits the data correctly.

The character of the distributions at all (four) observing frequencies (for the R- and L-polarization) were studied using both statistical methods. The main characteristics are summarized in Table 1. The χ^2 values are much greater than unity. Therefore, according to the statistical rules used our models are not consistent with the data. Nevertheless, the χ^2 values are lower for those models which in the detailed analysis were found to be

Table 1. Evaluation of the distribution type for all the spikes (whole interval lasting 16 minutes) using both methods.

freq. [MHz]	polarization	power-law fit: reduced χ^2	exponential fit: reduced χ^2
237	L	3.68	3.73
237	R	3.22	14.37
327	L	9.56	10.56
327	R	9.56	11.55
408	L	10.70	7.27
408	R	9.61	7.01
610	L	7.28	5.27
610	R	7.15	18.75

consistent with the data (see the following paragraphs). A loss of the model consistency for the data representing the global time intervals is not surprising, and might be caused, for example, by the variation of the minimum flux level at all studied frequencies.

3.2. Detailed study

A visual inspection of the recorded radio data reveals that the spikes had different intensities and were distributed with different rates. As the level of the minimum was varying in time, we selected for the further study some characteristic intervals that were studied in detail. In this study only the standard method was used, in order to remove the effects of the minimum flux variation occurred during long intervals. In Tables 2–6 the statistical parameters (starting time, maximum flux, maximum-minimum difference, cutoff and turnover, number of spikes, time rate of spikes, power-law index, reduced χ^2 function for the power-law and the exponential fits and type of distribution) corresponding to the spikes in the selected intervals at 237, 327, 408, 610 MHz are shown. In this detailed study we performed the analysis for sufficiently short intervals, i.e. 60 and 30 s (upper and lower parts of the mentioned tables). The results for both intervals are generally similar. However, for the longer time interval (60 s) the fitting reveals more definite results, i.e. a clear distinction between power-law and exponential fits.

For all distributions the cutoffs (the minimum radio flux plus 15%) and the turnovers were determined. These levels were used for the determination of the number of spikes and their rate of appearance. To determine the spike rate in the studied intervals the cutoff level proved to be more appropriate. Moreover, it turned out that for the power-law distributions the cutoffs and turnovers are nearly coincident, whereas for the exponential distributions there is a significant difference.

The spikes in all selected intervals and frequencies were designated according to their rates as: a) sparse spikes (less than 9 spikes s^{-1}, see Tables 2 and 3) and b) dense spikes (equal or more than 9 spikes s^{-1}, see Tables 4, 5 and 6). Examples of some typical distributions are shown in Figs. 2 and 3.

Summarizing all these results it turns out that the dense spikes and those with high intensities are distributed essentially in the exponential way, whereas the spikes with lower time rates

Table 2. Spike distribution parameters for the emission at 237 MHz, L-polarized data, for intervals lasting 60 and 30 s.

interval 60 [s]	**sparse spikes**
starting time [UT]	08:28:20
maximum flux [SFU]	220.02
max-min difference [SFU]	102.52
cutoff [SFU]	135.13
turnover [SFU]	134.80
number of spikes	514.00
rate of spikes [s^{-1}]	8.57
power-law: α	11.57
power-law: reduced χ^2	1.09
exponential: reduced χ^2	1.29
distribution type	power-law
interval 30 [s]	**sparse spikes**
starting time [UT]	08:28:20
maximum flux [SFU]	220.02
max-min difference [SFU]	102.52
cutoff [SFU]	135.13
turnover [SFU]	134.80
number of spikes	262.00
rate of spikes [s^{-1}]	8.73
power-law: α	13.63
power-law: reduced χ^2	0.90
exponential: reduced χ^2	0.89
distribution type	?

Table 3. Spike distribution parameters for the emission at 327 MHz, L-polarized data, for intervals lasting 60 and 30 s.

interval 60 [s]	**sparse spikes**		
starting time [UT]	08:23:20	08:28:20	08:30:40
maximum flux [SFU]	259.74	243.25	407.91
max-min differ. [SFU]	136.12	111.50	295.47
cutoff [SFU]	142.16	151.51	129.30
turnover [SFU]	147.43	151.90	126.98
number of spikes	536.00	368.00	440.00
rate of spikes [s^{-1}]	8.93	6.13	7.33
power-law: α	9.70	10.00	6.50
power-law: reduced χ^2	1.01	0.96	1.13
exponential: reduced χ^2	0.98	1.04	1.13
distribution type	?	?	?
interval 30 [s]	**sparse spikes**		
starting time [UT]	08:23:20	08:28:20	08:30:40
maximum flux [SFU]	235.28	219.58	248.99
max-min differ. [SFU]	108.72	86.46	132.98
cutoff [SFU]	145.54	153.09	133.41
turnover [SFU]	143.10	151.90	130.83
number of spikes	178.00	174.00	177.00
rate of spikes [s^{-1}]	5.93	5.80	5.90
power-law: α	14.66	9.90	6.01
power-law: reduced χ^2	1.19	0.99	0.97
exponential: reduced χ^2	1.55	1.09	1.08
distribution type	power-law	?	?

Table 4. Spike distribution parameters for the emission at 408 MHz, L-polarized data, for intervals lasting 60 and 30 s.

interval 60 [s]	**dense spikes**		
starting time [UT]	08:23:40	08:28:40	08:30:20
maximum flux [SFU]	441.97	336.48	764.34
max-min differ. [SFU]	337.02	222.81	657.61
cutoff [SFU]	120.69	130.72	122.74
turnover [SFU]	166.14	134.80	180.25
number of spikes	660.00	560.00	607.00
rate of spikes [s^{-1}]	11.00	9.33	10.12
power-law: α	4.08	3.85	2.30
power-law: reduced χ^2	1.30	1.26	1.35
exp: reduced χ^2	1.19	1.09	1.29
distribution type	exp	exp	?
interval 30 [s]	**dense spikes**		
starting time [UT]	08:23:56	08:29:10	08:30:40
maximum flux [SFU]	379.10	336.48	641.69
max-min differ. [SFU]	265.16	221.49	530.61
cutoff [SFU]	131.03	132.23	127.74
turnover [SFU]	210.97	156.51	200.00
number of spikes	337.00	270.00	309.00
rate of spikes [s^{-1}]	11.23	9.00	10.30
power-law: α	4.74	3.89	1.52
power-law: reduced χ^2	1.23	1.07	0.96
exp: reduced χ^2	1.24	1.03	0.91
distribution type	?	?	?

Table 5. Spike distribution parameters for the emission at 610 MHz, L-polarized data, for intervals lasting 60 and 30 s.

interval 60 [s]	**dense spikes**	
starting time [UT]	08:28:40	08:30:20
maximum flux [SFU]	1324.89	2751.59
max-min difference [SFU]	1086.25	2540.91
cutoff [SFU]	274.43	242.28
turnover [SFU]	487.17	436.60
number of spikes	721.00	703.00
rate of spikes [s^{-1}]	12.02	11.72
power-law: α	3.78	1.61
power-law: reduced χ^2	1.31	1.29
exponential: reduced χ^2	1.03	0.99
distribution type	exponential	exponential
interval 30 [s]	**dense spikes**	
starting time [UT]	08:29:10	08:30:24
maximum flux [SFU]	1324.89	2701.25
max-min difference [SFU]	1084.89	2490.57
cutoff [SFU]	276.00	242.28
turnover [SFU]	580.88	687.12
number of spikes	353.00	351.00
rate of spikes [s^{-1}]	11.77	11.70
power-law: α	3.60	2.46
power-law: reduced χ^2	0.67	1.05
exponential: reduced χ^2	0.58	1.03
distribution type	?	?

Table 6. Spike distribution parameters for the emission at 610 MHz, R-polarized data, for intervals lasting 60 and 30 s.

interval 60 [s]	**dense spikes**	
starting time [UT]	08:28:40	08:30:20
maximum flux [SFU]	2042.50	7401.48
max-min difference [SFU]	1760.23	7134.55
cutoff [SFU]	324.61	306.97
turnover [SFU]	663.23	861.98
number of spikes	721.00	702.00
rate of spikes [s^{-1}]	12.42	11.70
power-law: α	3.30	1.49
power-law: reduced χ^2	1.20	1.49
exponential: reduced χ^2	1.12	1.02
distribution type	exponential	exponential
interval 30 [s]	**dense spikes**	
starting time [UT]	08:29:10	08:30:24
maximum flux [SFU]	2042.50	7401.48
max-min difference [SFU]	1736.14	7134.55
cutoff [SFU]	352.32	306.97
turnover [SFU]	655.27	1484.21
number of spikes	361.00	346.00
rate of spikes [s^{-1}]	12.03	11.53
power-law: α	2.44	1.89
power-law: reduced χ^2	1.16	1.15
exponential: reduced χ^2	1.03	1.15
distribution type	exponential	?

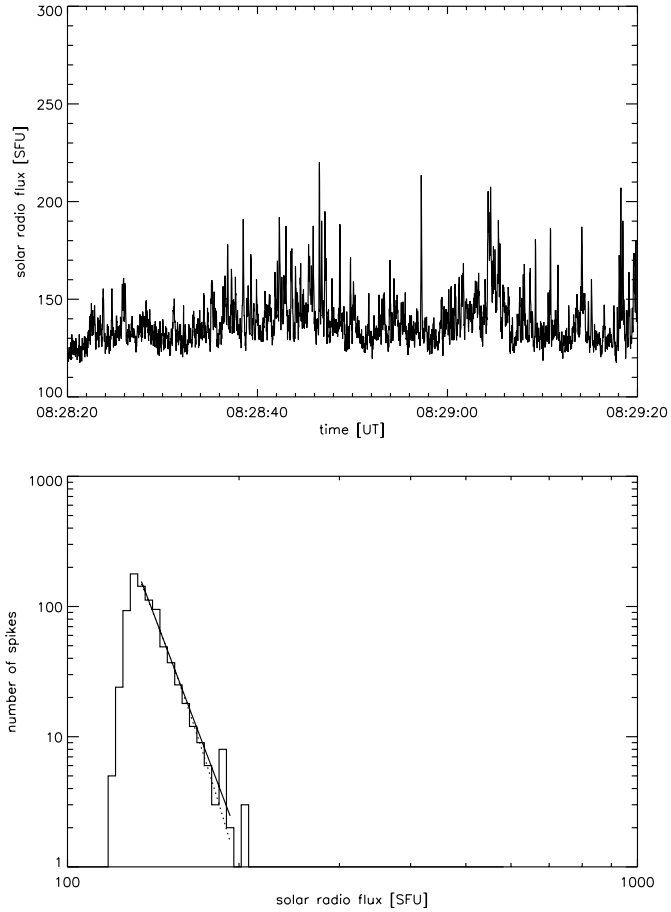

Fig. 3. Example of a 1 minute interval with sparse spikes observed at 237 MHz, L-polarized data, and the corresponding distribution. The solid line corresponds to the better fit: in this case power-law.

and lower intensities fit the power-law trend better. Moreover, the power-law exponents for the power-law distributions are higher ($\alpha \sim 6-15$) than those for the exponential distributions when they are fitted by power-law functions ($\alpha \sim 1.5-5$). Furthermore, more dense spikes were recorded at higher frequencies. However, comparing the rates at different frequencies during specified time intervals, we found similarities among these rates, at least at the two neighbouring frequencies.

Comparing the results of the detailed and the global study at different frequencies, we can see that at 237 MHz the spikes are weak and sparse in the whole 16 minute interval as well as in the selected short intervals. The results for the detailed studies generally show power-law distributions. On the other hand, at 408 and 610 MHz the spikes are strong and dense. The short interval analysis reveals exponential distributions. At 327 MHz the results are not definite, they seem to be a hybrid of the characteristics at 237 and 408 MHz.

3.3. Nonlinear analysis

Several papers deal with the fractal dimensions of solar dm-spikes (Isliker 1992; Isliker & Benz 1994a,b; Veronig et al. 2000). None of the studies reports finite dimension values for the analysed events. The papers of Isliker (1992) and Isliker & Benz (1994a,b) are based on correlation dimensions and use an extended dimension-estimate method. In the paper of Veronig et al. (2000), the local pointwise dimension method was applied in addition to the classical correlation dimension method. As discussed in this paper, the latter method has advantages above the classical correlation dimension calculation, since it can provide the basis for a non-invariant statistical description of the analysed time series, even in cases in which low-dimensional determinism cannot be established. Moreover, even if the retrieved dimension values do not represent the definite attractor dimensions of the system, they are still related to its degree of complexity, which makes them statistically meaningful specifically for comparative studies. Therefore we use in this paper the local dimension method, without claiming or supposing the presence of low-dimensional determinism in the analysed data sets.

We calculated the local pointwise dimensions for the L- and R-handed circular polarized components of each of the frequencies, 237, 327, 408 and 610 MHz. As the time series are quite long, 16 minutes covered by 48.000 points, we did not use all points of the time series for the calculation of the local dimension at point $x(t_i)$ but shifted a window of ± 2000 points around $x(t_i)$ through the time series. This still yields a reliable statistics in the calculation of the local dimensions but softens the influence of flux variations at longer time scales, which biases

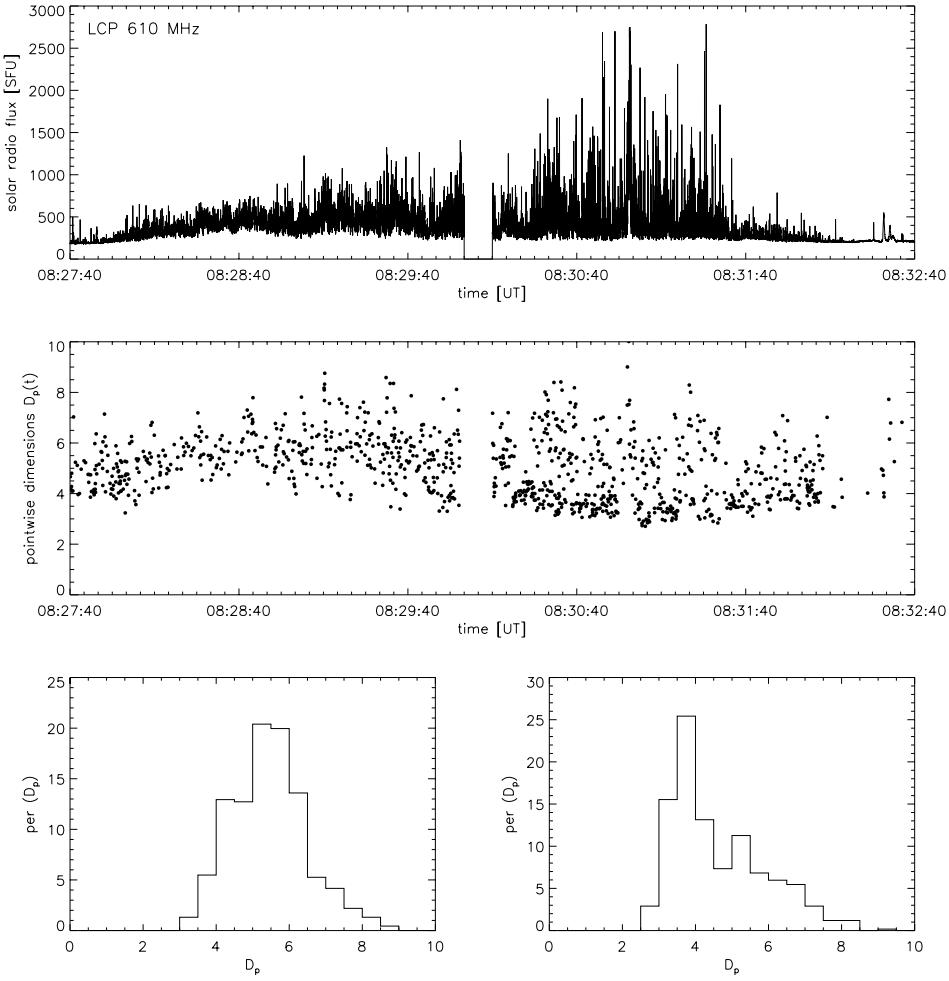

Fig. 4. Top panel: Time series of the L-polarized component at 610 MHz of the sub-interval 08:27:40−08:32:40 UT. Middle panel: The related pointwise dimensions $D_p(t_i)$. Bottom panels: The distributions of the dimension values, calculated for the two parts of the time series which are separated by the gap.

such kind of analysis based on distance measurements in phase space.

For each point $x(t_i)$ of the time series we calculated the related local dimension $D_p(t_i)$ for embedding dimension $m =$ 7–10. In a first step we determined the scaling region in the $\ln p_i(r)$ versus $\ln r$ curves to calculate the local dimension at point $x(t_i)$ as function of the embedding dimension, $D_p(t_i, m)$. In a second step the $D_p(t_i, m)$ were averaged over the selected embedding range $m = 7$–10 and tested for convergence. Points, for which the scaling regions did not show a distinct extension or the $D_p(t_i, m)$ did not converge with increasing embedding dimension, were rejected. The descriptions of the procedures, automatically testing for scaling and convergence behaviour, can be found in Veronig et al. (2000).

Fig. 4 shows the local dimensions of a sub-interval of the L-polarized component of the 610 MHz time series, from 08:27:40 to 08:32:40. This region is particularly suited for the dimension analysis as the spike frequency is very high and the series is not interrupted by quiet phases. The picture is mainly the same for all the frequencies, L- as well as R-polarized components. Only for the 237 MHz time series the statistics of spikes turned out to be too poor to carry out a reliable dimension analysis. The bottom panels of Fig. 4 show the histograms for the local dimensions for the two parts of the depicted time series separated by the gap, the behaviour is quite different. The distribution of the dimension values calculated for the sub-interval 08:27:40−08:30:00 has its center at rather high values, D_p around 5 to 6, and shows a quite symmetric characteristics. However, the dimension histogram for the sub-interval 08:30:10−08:32:40 has a distinct peak at D_p values around 3 to 4, with an asymmetric extension to higher values.

Fig. 5 shows the time evolution of the pointwise dimensions for the same subsection in detail, as for each 30 s sub-interval the histogram of the dimensions is plotted. It is clearly visible that starting at around 08:29:40 the distribution of the dimension values becomes more and more asymmetric and a kind of "sub-population" of spikes with low dimension values, $D_p < 4$, develops. This feature is particularly evident in the interval 08:31:10−08:31:40, and afterwards removes rather fast. The same scenario appears also at the other frequencies where the dimension analysis could be applied successfully, i.e. at 327 and 408 MHz.

In Fig. 6 the percentage of spikes belonging to this "sub-population", defined as spikes with dimension values $D_p < 4$, is plotted versus time. The top panel shows the scenario for the L-components, the bottom panel for the R-components. The re-

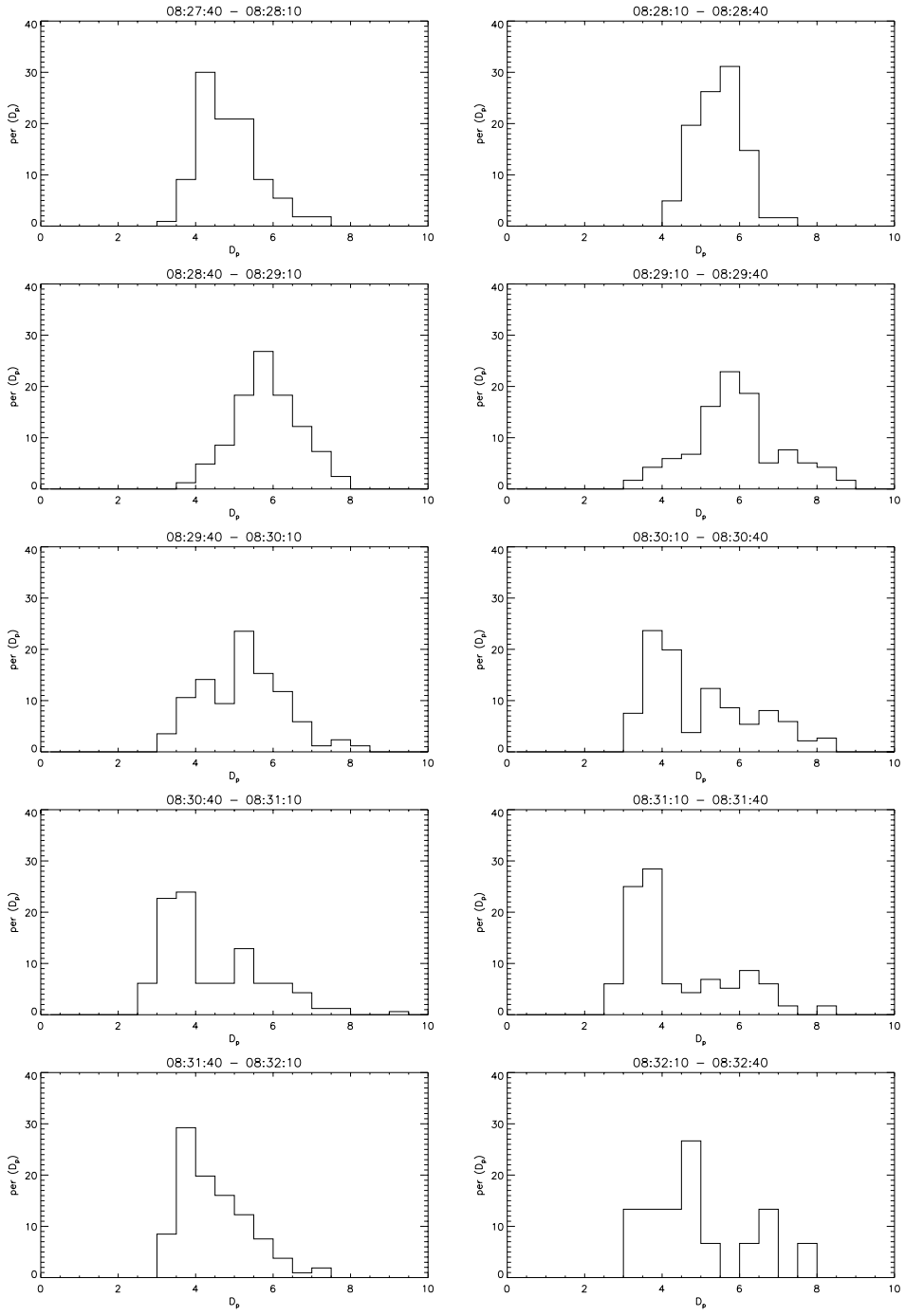

Fig. 5. Time evolution of the distribution histograms of the dimension values $D_p(t_i)$ for the L-polarized 610 MHz series, ranging from 08:27:40 to 08:32:40. The histograms of the dimensions are built up for each 30 s sub-interval.

markable increase of the number of spikes with low dimension values takes place at all considered frequencies, and no significant difference for the two polarization components is detectable. However, at higher frequencies the phenomenon seems to be stronger and it reaches its maximum slightly earlier.

For the analysis of recurrence plots, we divided each of the time series into sub-intervals covering 30 s and for each of these intervals recurrence plots were built up for various embedding dimensions m. Fig. 7 shows the recurrence plots for two different sub-intervals of the 408 MHz series (L-component). If points $\boldsymbol{\xi}_i$ and $\boldsymbol{\xi}_j$ are near neighbours in the reconstructed phase space, there is a dot at position (i, j) in the recurrence plot. In the plots shown in Figs. 7 and 8 we defined as nearest neighbours the 0.2% nearest points. The diagonal is trivially filled with dots, as $i = j$.

The recurrence plots shown in Fig. 7 are related to sub-intervals in the L-polarized 408 MHz time series (08:28:10−08:28:40 and 08:28:40−08:29:10) before the distribution of the local dimensions shifts to smaller values. The recurrence plots shown in Fig. 8 are related to sub-intervals (08:30:40−08:31:10 and 08:31:10−08:31:40), in which the proportion of dimension values $D_p < 4$ reaches its maximum.

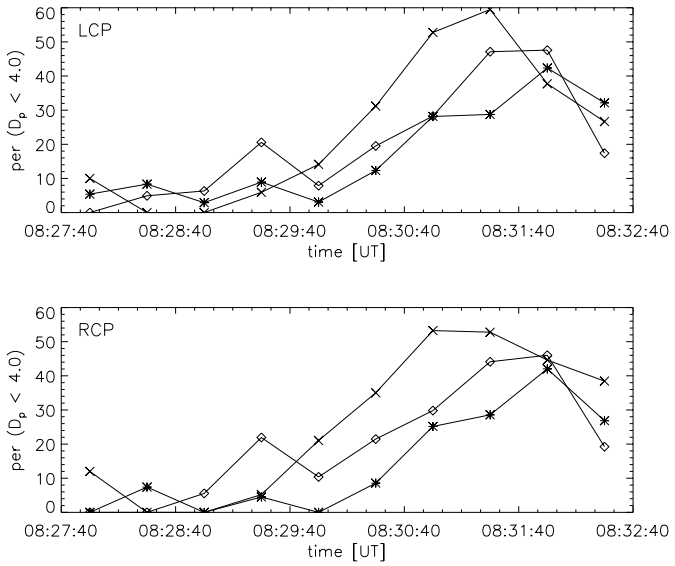

Fig. 6. Time evolution of the percentage of dimension values $D_p < 4$, top panel: for the L-polarized components, bottom panel: for the R-polarized components. Asterisks are related to 327 MHz, diamonds to 408 MHz, and crosses to 610 MHz.

Comparing the recurrence plots relevant to different time intervals, a quite significant change becomes evident. This aspect is qualitatively the same for all the considered frequencies and both polarizations. The two recurrence plots in Fig. 7 reveal just a few lines parallel to the diagonal which are indicative of finite local Lyapunov exponents. Moreover, there are only a few dots present in regions far away from the diagonal, revealing an underlying drift. The recurrence plots in Fig. 8 show significantly longer lines parallel to the diagonal than the recurrence plots related to previous time intervals. This means that for the sub-intervals shown in Fig. 8 the local Lyapunov exponents are smaller, indicating that the exponential divergence rate of nearby trajectories is smaller and the time of predictability is longer than in the earlier sub-intervals.

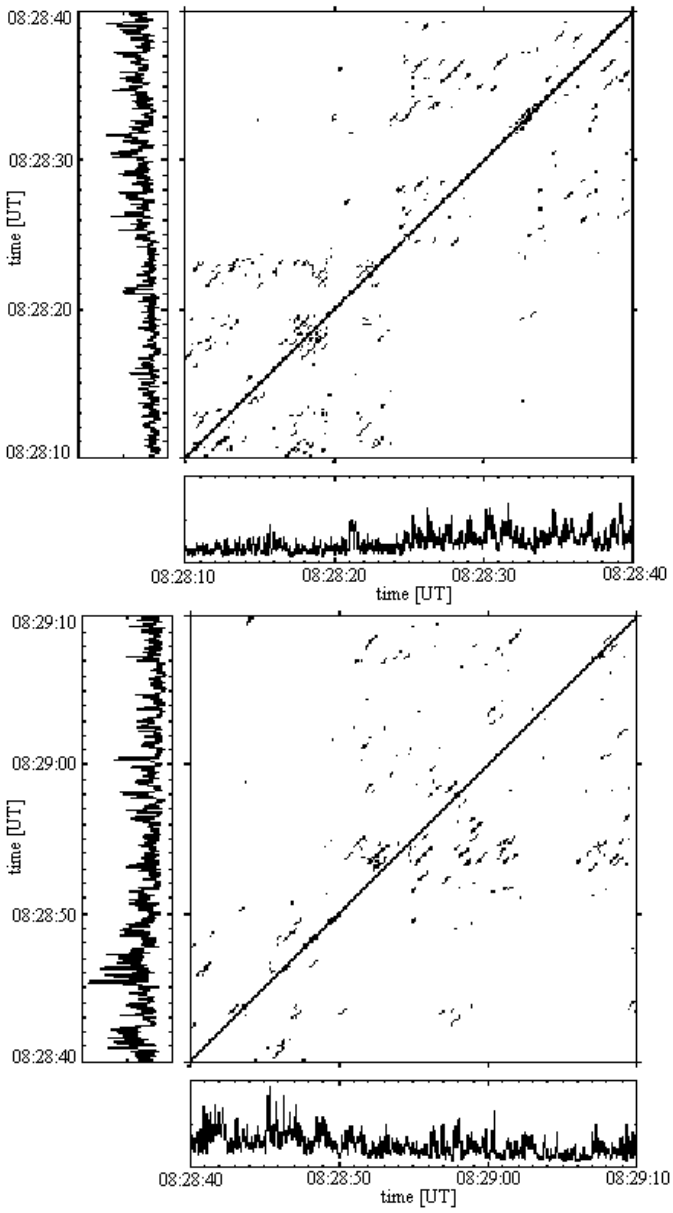

Fig. 7. Recurrence plots for two sub-intervals of the 408 MHz time series (L-polarized component), each covering 30 s. To clarify the correspondence between time series and recurrence plot, the related interval of the time series is plotted along the horizontal as well as the vertical direction of the recurrence plot.

3.4. Interpretation of the nonlinear analysis results

The dimension as well as the recurrence plot analysis reveals a distinct change in the behaviour of the related statistical quantities at the same time epoch, culminating around 08:31:30. The dimension values shift to significantly smaller values, $D_p < 4$, the recurrence plots become more regular, showing longer lines parallel to the diagonal, which are indicating smaller local Lyapunov exponents. An interpretation of these types of behaviour in terms of nonlinear dynamics theory means that the degree of chaos of the system seems to decrease during its time evolution, since the dimensions as well as the leading Lyapunov exponents develop to smaller values.

The occurrence of rather high local dimension values could be caused by a situation, in which different "populations" of spikes are acting in the same time series; these different populations might be related, for instance, to different sources or different propagation conditions. Different emission processes are not probable, as we do not observe any change in the spikes parameters, such as polarization, duration, and delay between polarimetric components. When in the sequence of time one kind of spike population becomes dominant, this would be reflected in the analysis as a change to lower dimension values, indicating that the degree of freedom of the overall system became lower. All such kinds of details can be recognized in Fig. 6, which is exemplary for the time evolution of the dimension values for the different frequencies and polarizations (except 237 MHz). Analogously for such a situation also the Lyapunov exponents would

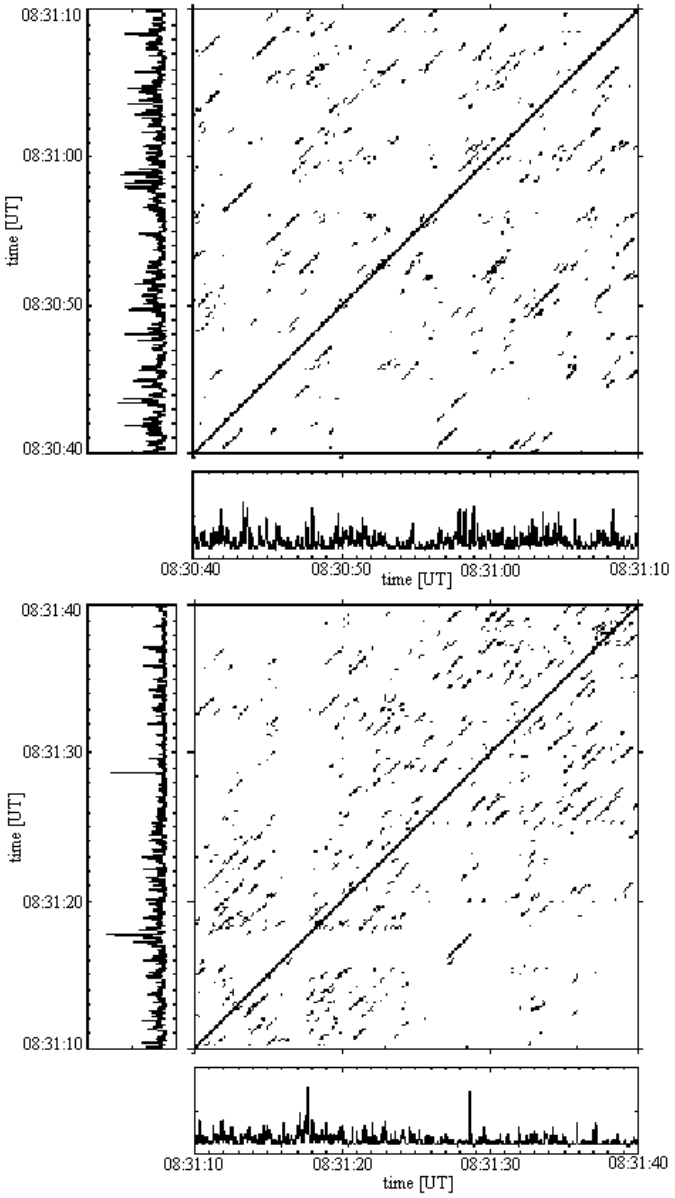

Fig. 8. Recurrence plots for two sub-intervals (in which the proportion of dimension values $D_p < 4$ reaches its maximum) of the L-polarized 408 MHz time series, each covering 30 s.

evolve from high values, representing the compound system, to lower values for one single system being dominant, which can be seen in Figs. 7 and 8.

Zlobec & Karlický (1998) carried out a statistical analysis of the same spike series, where CW and ACW cases were discriminated. CW (ACW) means clock-wise (anti-clock-wise) sense of the loop in the R−L versus R+L plots when the data of a single spike are considered according to the time sequence. The presence of such a loop is determined by the delay of the weaker (stronger) polarimetric component in respect to the other one. In their analysis it turned out that the ratio of CW to ACW spikes, which initially was not far from unity, changed remarkably in the interval 08:30:30−08:32:00 with the maximum at around 08:31:30. These changes in the CW/ACW ratio were interpreted as an alteration in the propagation conditions in the solar corona. At the same time interval we reported a remarkable change in the distribution of the dimension values and the local Lyapunov exponents, both tending to smaller values. Even if the dimension distribution changes are the strongest at 610 MHz (Fig. 6) but the CW/ACW changes are the most remarkable at 408 MHz (Zlobec & Karlický 1998, Fig. 8), the coincidence in the time evolution of the graphs for the dimension values $D_p < 4$ and for the CW/ACW ratio turns out to be quite striking.

All these statistical methods, dimension analysis, recurrence plots, CW/ACW investigations, show coincidently a remarkable change at the same time, i.e. at about 8:31.

4. Discussion and tests

The question arises why the character of the spike distribution changed from power-law to exponential as function of the spike rate and intensity increase. Let us mention that in the paper by Aschwanden et al. (1998) exponential distributions were found in most cases (95%). This fact is in contrast with the coherent emission mechanism and was explained by Aschwanden et al. (1998) as a consequence of a saturation process at a fixed amplification factor for all the spikes.

Analyzing our data we realized that sparse spikes (case with low rates and low intensities) are related to the power-law distributions in agreement with the theory of coherent mechanisms expected for spikes. Let us discuss now the possible causes that could generate the preferred exponential distribution for high spike rates. The first possibility is connected with the observations: a) superposition of spikes and b) insufficient time and frequency resolution. The second possibility is related to the physical processes in the spike sources, mainly when these sources are not independent, i.e. there are some interactions among them. To make a decision among these possibilities we applied several tests, which are described in the following subsections.

4.1. Superposition of spikes

We tried to test the first possibility as follows: starting from the case (at 237 MHz, L-polarization) in which the observed spikes were distributed according to the power-law we introduced an artificial superposition of spikes. On the original data above the cutoff (minimum plus 15%) we superimposed the same data after the introduction of a time delay from 1 to 6 points (i.e. time interval 0.02−0.12 s). This time delay is similar to the spike duration. It is interesting to recall that the mean spike duration (at half power) was 0.092 ±0.020 s at 237 MHz, 0.077 ±0.015 s at 327 MHz, 0.052 ±0.009 s at 408 MHz, and 0.040 ±0.003 s at 610 MHz (Zlobec & Karlický 1998). For comparison, the inverse of the maximum spike rate (12 s^{-1}) is 0.0833 s, therefore most of the spikes were probably single ones.

After the superposition we analysed the type of distributions in the artificial data sets. The distributions reveal that their power-law character is conserved (see Fig. 9).

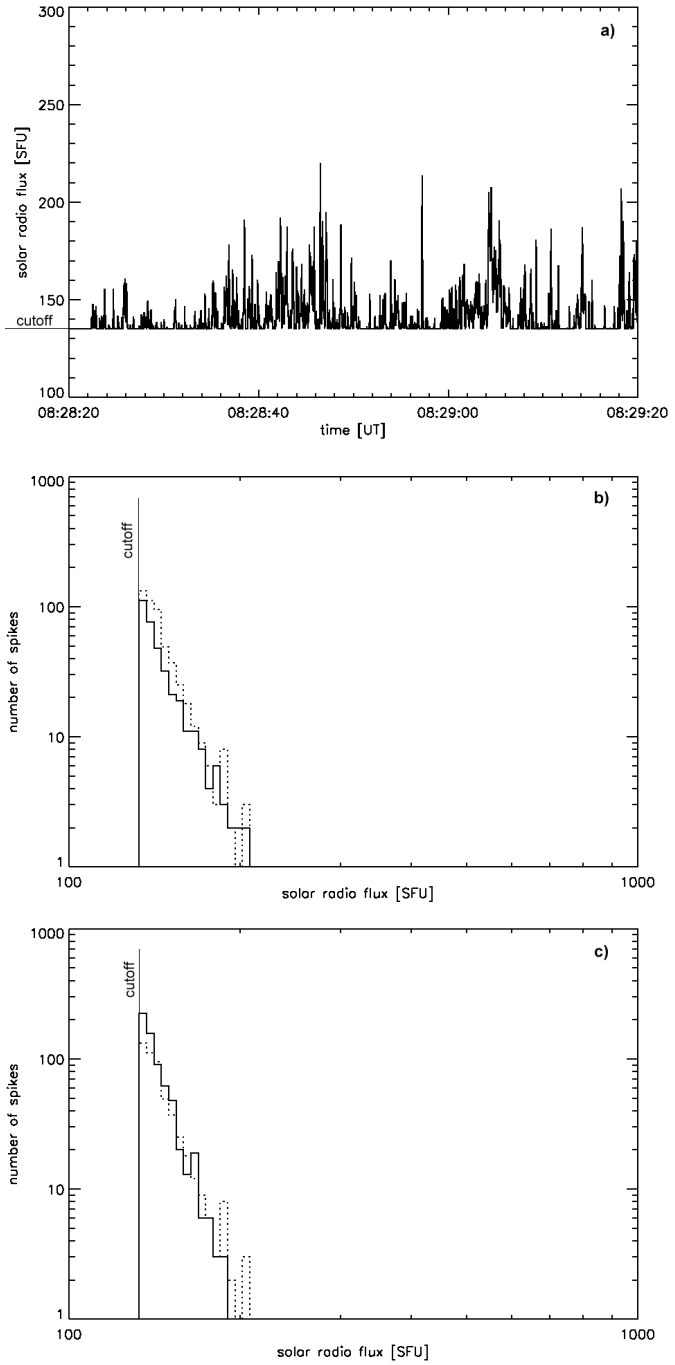

Fig. 9a–c. Results of the first test with spike superposition (see also Table 7). **a** Radio flux at 237 MHz, L-polarized data above the cutoff value. **b** Distribution of the original data set (dotted line) and normalized distribution of the artificial data set with a 1-point time-delay (solid). **c** Distribution of the original data set (dotted line) and normalized distribution of the artificial data set with a 4-points time-delay (solid).

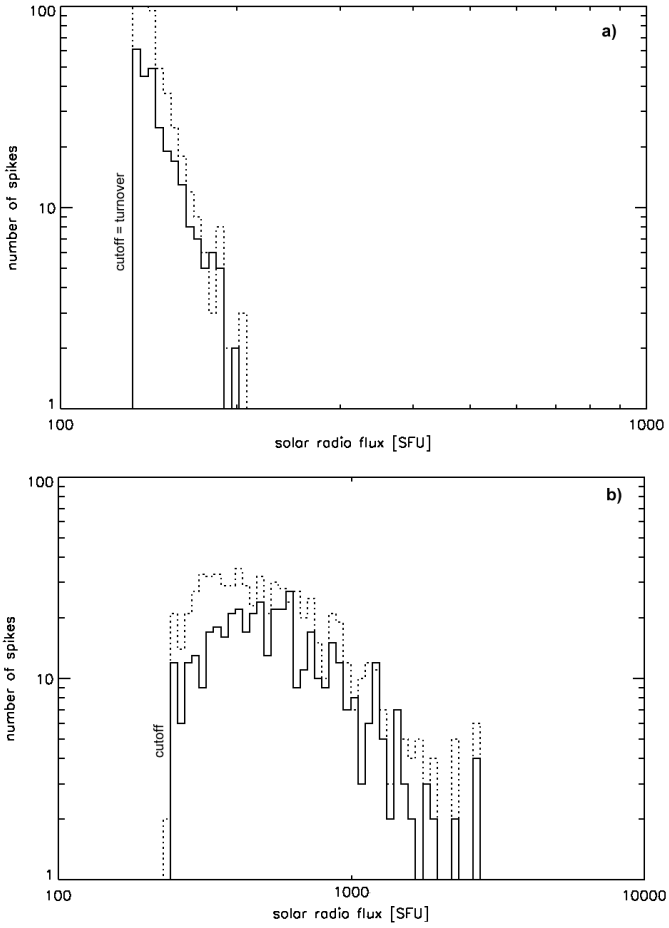

Fig. 10a and b. Examples of the second test with lower sampling rate: **a** Distribution of spikes observed at 237 MHz, L-polarized data, 1 minute interval (dotted line) and normalized distribution of spikes having the sampling interval two times longer than that of the original (solid line). **b** Distribution of spikes observed at 610 MHz, L-polarized data, 1 minute interval (dotted line) and normalized distribution of spikes having the sampling interval two times longer than that of the original (solid line).

4.2. Insufficient time and frequency resolution

Furthermore, using the same data sets with power-law distribution and another one with exponential distribution (at 610 MHz, L-polarization) we tried to test also the effects of insufficient time resolution by decreasing artificially the sampling rate by a factor two and three. Even in this experiment no essential change of the distribution type was found (see Fig. 10, upper part for the power-law distribution and bottom part for the exponential one).

4.3. Distribution type versus spikes intensities

The power-law distributions were preferentially found for low-intensity spikes. On the other hand, high-intensity spikes are fitted better by exponential distributions. Thus, the question about the distribution type dependence on the spikes intensity arises. Therefore, we studied the problem for low-intensity spikes in a time interval where also high-intensity spikes were observed.

For comparison with the L-polarized 237 MHz spikes having power-low distribution, we chose the L-polarized 408 MHz spikes in the sub-interval 08:28:20−08:29:20. Here we chose

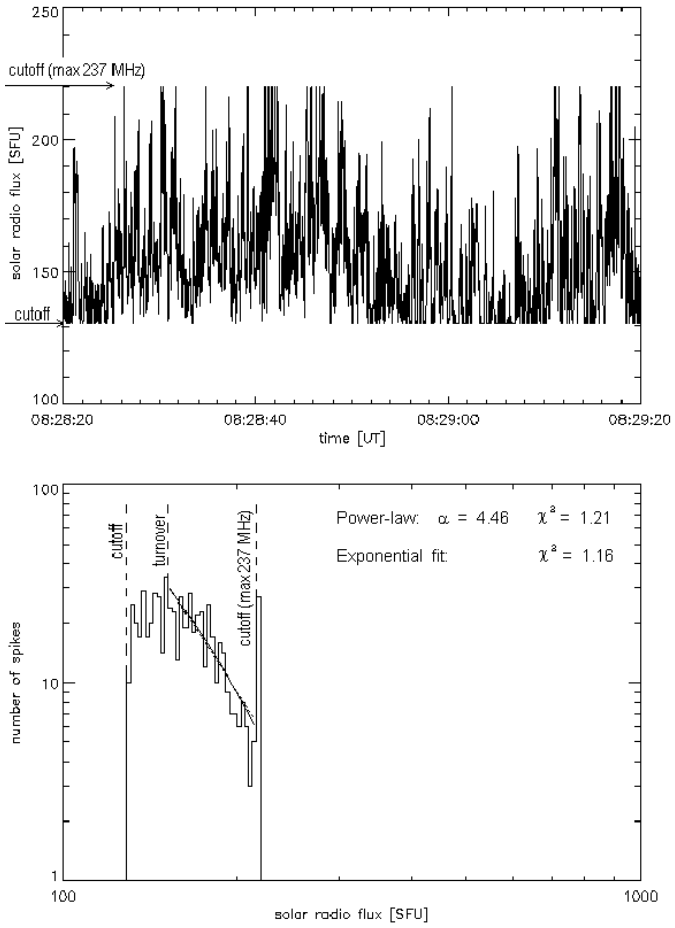

Fig. 11. Examples of the third test with cut spikes: in the top panel we report the spikes observed at 408 MHz, L-polarized data, 1 minute sub-interval, where the cutoff (max 237 MHz) is equal to the maximum flux at 237 MHz (L-polarized data) during the same time sub-interval. The corresponding distribution is given in the bottom panel. The solid line corresponds to the better fit: in this case exponential.

the intensity range corresponding to that of the 237 MHz spikes (135−220 SFU), and determined the distribution type in this range (see Fig. 11 and Table 7). The resulting distribution type is fairly close to the exponential distribution, i.e. the same trend as for the complete intensity range. This indicates that the distribution type does not change due to the lowering of the intensity interval.

5. Conclusions

Although it is difficult to make fully convincing tests, the present results indicate that the change of the distributions as a function of the spike density and intensity increase, has its origin in the sources of spike generation or in propagation conditions. We suggest that the group of spikes with low rates and intensities represents a group of independent and isolated events. In this case the frequency distribution is power-law, in agreement with the coherent mechanisms of spike emission. On the other hand the situation changes when the rate of spikes and their intensity are high enough, since the phenomena do not remain independent. The spikes probably undergo a mutual interaction in their sources and thus influence the amplification at the time of their generation as suggested by Aschwanden et al. (1998).

Table 7. Statistical parameters for cut spikes with cutoff (max 237 MHz) of 408 MHz L-polarized data. The distribution remains exponential. The time interval lasts 60 s.

interval 60 [s]	**dense spikes**
starting time [UT]	08:28:20
original maximum flux [SFU]	336.478
cutoff(max 237 MHz) [SFU]	220.024
cutoff(max 237 MHz)-min difference [SFU]	106.353
cutoff [SFU]	130.722
turnover [SFU]	151.033
number of spikes	610.00
rate of spikes [s^{-1}]	10.17
power-law: α	4.46
power-law: reduced χ^2	1.21
exponential: reduced χ^2	1.16
distribution type	exponential

A further interesting aspect is that in the late phase of the spike emission the degree of their complexity is sharply decreasing. Comparing the distributions of the spikes at this time with those at earlier intervals, we found that both distributions are better fitted by exponential functions than by a power-law. Nevertheless, for the power-law fits we found that their exponent decreases at the time of low complexity degree (see e.g. exponents α = 3.78 and 1.61 in Table 5). It turns out that at this time interval strong spikes are more numerous than before. These results seem to reveal further aspects of the fixed amplification factors for strong spikes as suggested by Aschwanden et al. (1998). However, a further verification of the distribution behaviour for spikes is necessary. Moreover, we cannot exclude the possibility of a change in the propagation conditions as well.

Acknowledgements. H.M. thanks Markus J. Aschwanden for stimulating discussions about the χ^2 statistics. H.M. and M.K. acknowledge the support through the key projects K1-043-601 and the grant A3003707 of the Academy of Sciences of the Czech Republic. M.M. and P.Z. acknowledge the support of the Italian Space Agency (ASI) and the Ministry for University and Research (MURST). A.V. acknowledges the support of ASI.

References

Abarbanel H.D.I., 1996, Analysis of Observed Chaotic Data. New York: Springer
Akimov V.V., Ambrož P., Belov A.V., et al. 1996, Solar Phys. 166, 107
Aschwanden M.J., 1990, A&AS 85, 1141
Aschwanden M.J., Dennis B.R., Benz A.O., 1998, ApJ 497, 972
Benz A.O., 1986, Solar Phys. 104, 99
Benz A.O., Csillaghy A., Aschwanden M.J., 1996, A&A 309, 291
Bevington P.R., 1969, Data Reduction and Error Analysis for the Physical Sciences. New York: McGraw-Hill
Eckmann J.P., Oliffson Kamphorst S., Ruelle D., 1987, Europhys. Lett. 4/9, 973
Fleishman G.D., Yastrebov S.G., 1994, Solar Phys. 154, 361

Fraser A.M., Swinney H.L., 1986, Phys. Rev. A 33, 1134
Grassberger P., Procaccia I., 1983, Phys. Rev. Lett. 50, 346
Grassberger P., Schreiber T., Schaffrath C., 1991, Int. J. Bifurcation and Chaos 1, 521
Holman G.D., Eichler D., Kundu M., 1980, in Kundu M., Gergely T. (eds.), IAU Symp. 86, 465
Isliker H., 1992, Solar Phys. 141, 325
Isliker H., Benz A.O., 1994a, A&A 285, 663
Isliker H., Benz A.O., 1994b, Space Sci. Rev. 68, 185
Kantz H., Schreiber T., 1997, Nonlinear Time Series Analysis, Cambridge: University Press
Karlický M., 1984, Solar Phys. 92, 329
Karlický M., 1992, in: Švestka Z., Jackson B.V., Machado M.E. (eds.), Eruptive Solar Flares. Springer-Verlag, 399, 171
Karlický M., Sobotka M., Jiřička K., 1996, Solar Phys. 168, 375
Kuijpers J., Van der Post, Slottje C.P., 1981, A&A 102, 331
Melrose D.B., Dulk G.A., 1982, ApJ 259, 844
Press W.H., Flannery B.P., Teukolsky S.A., Vetterling W.T., 1992, Numerical Recipes. Cambridge: University Press
Schwarz U., Benz A.O., Kurths J. et al., 1993, A&A 277, 215
Slottje C., 1981, Atlas of Fine Structures of Dynamic Spectra of Solar Type IV-dm and some Type II Radio Bursts, Dwingeloo Observatory
Schreiber T., 1999, Phys. Rep. 308, 1
Stähli M., Magun A., 1986, Solar Phys. 104, 117
Takens F., 1981, in: Rand D.A., Young L.S. (eds.), Dynamical Systems and Turbulence. Berlin: Springer, 366
Theiler J., 1986, Phys. Rev. A. 34, 2427
Tajima T., Benz A.O., Thaker M. et al., 1990, ApJ 353, 666
Veronig A., Messerotti M., Hanslmeier A., 2000, A&A 357, 337
Wentzel D.G., 1991, ApJ 373, 285
Zlobec P., Karlický M., 1998, Solar Phys. 182, 477